Integrating MEMS IMU with GNSS for Vehicle Navigation

Chad LY and John OGUNDARE, Canada

Commissions: 5 – Positioning and Measurement, 6 – Engineering Surveys

Key words: MEMS, IMU, GNSS, INS, Low Cost, Vehicle Navigation, Kalman Filter, Loosely-Coupled, GNSS – INS Integration, Autonomous Navigation, Coordinate Frames

Summary

This study is an attempt at integrating MEMS IMU with single-frequency GNSS receivers and developing an algorithm to solve positioning as a two-dimensional problem as a simplification of what is essentially three-dimensional. The integration of Lord MicroStrain 3DM-GX5-10 IMU with single frequency multi-constellation GNSS done in this study was based on a loosely-coupled Kalman filtering algorithm. Two approaches are followed in orienting the track of the navigating vehicle: using the immediate past bearing estimates from GNSS measurements for subsequent iterations and using the magnetometer measurements. The general results obtained showed that the loosely-coupled Kalman Filter algorithm favoured the accuracies of the IMU measurements more than the GNSS solutions. Although the results in this study did not compare very well with those based on only GNSS, it is demonstrated that two-dimensional integration algorithm can still be relied on at the moments of satellite downtime. Due to limited resources, a longer track could not be run to assess the quality of the INS used in this project. People looking to further this work should consider integrating the GNSS and IMU using a tightly-coupled method and implementing the more rigorous three-dimensional algorithm.

Integrating MEMS IMU with GNSS for Vehicle Navigation

Chad LY and John OGUNDARE, Canada

1. INTRODUCTION

Global Navigation Satellite System (GNSS)-based positioning and navigation have revolutionized many industries (e.g. surveying and navigation) since the introduction of the first GNSS, Global Positioning System (GPS) (El-Rabanny, 2006, p. 11). GNSSs offers greater satellite availability, higher precision and reliability. However, due to some sources of errors (mainly external), the computed position solution is usually not always accurate without some corrections being applied. In addition, GNSS solutions are only available when satellite visibility is not interfered with, otherwise this will create periods of time where position is not available. The potential solution to this is to integrate GNSS with inertial measurement units (IMUs), which will provide positions during times of GNSS position down-time. In this case, the IMUs will use the dynamic motions of the vehicle, which they measure to calculate the positions of the vehicle given a known starting position. Although IMUs are capable of providing some solutions to the positioning problem without GNSS, their solutions, however, are subject to some internal biases that degrade accuracies without bound over time (Grewal, Weill, & Andrews, 2001, p. 1). When an IMU and a GNSS are integrated, they form a system usually called inertial navigation system (INS).

1.1 Background

IMUs are electronic devices that sense specific forces such as linear acceleration, angular rate and magnetic fields. Traditionally, IMUs were used for military, scientific and commercial aircraft applications due to the cost of high-quality sensors and need for a stabilized sensor platform. However, advances in material processing have made small, low-cost inertial sensors (solid state and micromechanical) possible. This technological development is referred to as a micro-electro-mechanical system (MEMS), which is a technology of microscopic devices made of thin layers of metals and insulators in combination with silicone. These MEMS based IMUs have a reduced acuracy and precision when compared to ”normal” IMUs, but opens more options for low-cost, commercial navigation applications especially when integrated with GNSS receivers. This integration allows for on-line calibration and error estimation (Farrell & Barth, 1999, p. ix). As the errors from IMUs are internal and the errors from GNSS are external, the integration of the two systems are to complement each other.

This study is an attempt at integrating MEMS IMU with single-frequency GNSS receivers and developing an algorithm to solve positioning as a two-dimensional problem as a simplification of what is essentially three-dimensional. Moreover, a strap-down approach was implemented to mitigate costs and simulate a realistic scenario of the integration being used for commercial vehicle navigation. Towards the goal of this study, certain assumptions and simplifications are made regarding the integration process.

1.2 Assumptions and Simplifications

To simplify a traditionally three dimensional INS to a two dimensional one, certain assumptions must be made. Typically, the influence of gravity affects accelerometer measurements along the z-axis, where the sensed value would have to be multiplied by the gravitational constant in order to obtain a metric measurement. However, since a two dimensional coordinate system is assumed, gravity no longer affects accelerometer measurements; therefore, altitude, pitch and roll are assumed to be zero. Due to the sensitivity of the sensors, Coriolis effect is usually accounted for. Coriolis effect is the inertial force that acts on objects that are in motion within a reference frame. An example of this would be the rotation of earth; however, the low accuracy of this project allows for Coriolis effect to be ignored. The expected GNSS accuracy is assumed to be at 5 meters at a 68% probability level (one standard deviation) under the assumption that the accuracy of a GNSS solution is a tenth of the wavelength the satellite signal emits (Hofmann-Wellenhof & Moritz, 2006, pp. 179,184). Also, the initial position and velocity are assumed to have no correlation with initial velocity being assumed to be 0 m/s.

2. SYSTEMS OVERVIEW AND ERROR SOURCES

2.1 Global Navigation Satellite Systems

In modern day, satellites from any of the GNSS can be used to accurately position objects. This is done by determining the position of an antenna connected to a GNSS receiver where the antenna would be over the desired point. The position of the antenna is calculated in a common coordinate system, which is typically in an Earth Centered Earth Fixed (ECEF) reference frame. Propagated into the GNSS position solutions are several types of errors and biases, which are systematic and random in nature. The sources of these errors are from the GNSS receivers, satellites and the atmosphere. The errors originating from the satellite include ephemeris errors and satellite clock errors. Ephemeris errors are due to the imperfect modeling of satellite orbital motions resulting in errors of estimated satellite positions. Satellite and receiver clock errors are due to the systematic bias within the satellite/receiver clock's ability to accurately and consistently measure epochs of time (El-Rabanny, 2006, pp. 47-48). The clock bias and drift, however, is recorded in the satellite's navigation message and can later be used in the post-processing phase to correct the error. The errors originating from the atmosphere include signal multipath, ionospheric and tropospheric delays. Signal multipath is the degradation of satellite signals before they are measured by the receiver. The degradation comes from the signal being reflected off different surfaces before it is measured by the receiver. Ionospheric delay is due to the charged particles in the ionosphere resulting in errors in horizontal position once measured by the receiver. Tropospheric delay is due to the dry and wet components of the atmosphere resulting in a vertical positioning error once it is measured by the receiver (El-Rabanny, 2006, pp. 43-56).

2.2 MEMS IMU

The Lord MicroStrain 3DM-GX5-10 used in this study is a low-cost IMU with three types of MEMS sensors: accelerometer, gyroscope and magnetometer. The scope of this project required only two of these sensors to be used (accelerometer and gyroscope). The

accelerometer senses linear acceleration in three orthogonal coordinate axes, where the coordinate axes in a two-dimensional plane are considered for this study. Accelerometer sensors are sensitive enough to detect the influences of gravity on the instrument and are typically used to calculate pitch and roll, and add redundancy to orientation. The gyroscope senses angular rate in radian per second in three orthogonal coordinate axes, and angles are measured with reference to the local geodetic frame. The IMU also measures magnetic heading (the bearing with reference to magnetic north), which can be used to orient measurements after applying grid declination.

While IMUs have high accuracies during initial periods of measurements, the accuracies quickly degrade without bound over time due to internal biases. There are two types of biases that affect the sensors within the IMU; bias instability and initial bias error. Bias instability is the rate of which a sensor's measurements deviate from its mean value of the output. This bias is the random error associated with that specific sensor and represents how stable the sensor is over a specified period of time. Initial bias error is the constant error in a sensor's measurements. This is a systematic error that can be removed by using it as correction to the measurements. The sample bias specifications for the Lord MicroStrain 3DM-GX5-10 used in this study are given in Table 1.

Table 1 Manufacturer's specifications showing the bias of the sensors.

Output	Accelerometer	Gyroscope
Bias Instability	± 0.04 mg	8°/hr
Initial Bias Error	± 0.002 g	± 0.04°/sec

3. COORDINATE FRAMES

Since INS and GNSS measurements are being made relative to different coordinate systems, it is important to understand how to bring all of the measurements to the same coordinate system. For the purpose of this study, five coordinate frames are considered: Earth-Centered Earth-Fixed, Local Geodetic, Body, Platform, and Instrument.

3.1 Earth Centered Earth Fixed Frame

The origin of this frame is fixed to the center of the earth with the axes rotating relative to the inertial frame due to the daily rotation of earth and yearly revolution about the sun. The z-axis is aligned with respect to the Earth's spin axis along the Conventional Terrestrial Pole (CTP); the x-axis is oriented along the International Earth Rotation and Reference Systems Service (IERS) reference meridian defining the zero longitude (Greenwich Meridian); and the y-axis is oriented with respect to the x and y, forming orthogonal right-handed three-dimensional system. GNSS measurements are typically made in relation to this frame. The earth's geoid is usually approximated as an ellipsoid, a consistent mathematical surface representing the earth's shape.

3.2 Local Geodetic Frame

The origin of the local geodetic frame is at the instrument location on a tangent plane to the geodetic reference ellipsoid. The tangent plane is attached to the instrument location on the surface of the earth for local measurements. The x-axis points to true north and the y-axis is orthogonal to the x-axis pointing east. The z-axis completes the right-handed coordinate system. This frame is the north (x), east (y), down (z) rectangular coordinate system that is often seen. In this study, the UTM zone 10 map projection grid system is considered as equivalent to this system, and was used in the integration process.

3.3 Body Frame

The body frame is the vehicle frame, describing the object that is navigating. In an INS, the objective is to determine the position of the vehicle based on the measurements collected from the various sensors attached to the sensor platform aboard the vehicle. The origin of this frame is the center of mass of the vehicle (which may correspond with the origin of the local geodetic frame), while the x-axis is defined as the forward direction, the z-axis points towards the bottom of the vehicle (along the direction of gravity), and the y-axis completes the orthogonal, right-handed coordinate system.

3.4 Platform Frame

A strap-down platform was attached to the vehicle, where the coordinate axes are the same as the body frame coordinate axes. The origin of the platform frame is the center of the platform (where the IMU is attached).

3.5 Instrument Frame

Inertial sensors within the instrument sense specific forces applied to the instrument in relation to the instrument's coordinate frame. These inertial sensors' coordinate axes are aligned with the instrument axes. The instrument axes are nominally aligned with the platform axes.

4. FIELD TESTS AND DATA COLLECTION

Field test runs were carried out in Coquitlam, B.C., Canada in September 2019. The IMU was strapped-down to the center of the platform frame to align the two coordinate frames. Since the origin of the body frame can arbitrarily be placed, it is set in the same position as the center of the IMU. Along the x-axis of the IMU, two GNSS receivers are strapped-down onto the platform with taped distances measured between each GNSS receiver to the center of the IMU. The platform setup showing the strapped-down instruments is shown in Figure 1. With this arrangement, all measured quantities should theoretically refer to the same origin (center of the IMU).

A base station was set nearby the project area to broadcast base corrections to one of the GNSS receivers for Real Time Kinematic (RTK) solution. The Lord MicroStrain 3DM-GX5-10 required "MIP Monitor" software to run and control the IMU settings. The alterable settings in the software allowed operators to change data capture rate, quantities measured,

filters applied, GNSS constellations, and more. The IMU was set to record accelerometer and gyroscope measurements at 50 Hz. The IMU's GNSS was set to record at 1 Hz and measured to the same satellites as the GNSS receiver getting base corrections. A track was driven with all instruments on the platform measuring simultaneously.

The outputted sensor measurements are recorded in a comma-separated values (CSV) file. The contents of the file, however, is based on the sensor menu items selected by the operator prior to conducting the field tests. In this study, the IMU was set to sense and record accelerometer and gyroscope measurements at 50 Hz and the IMU's GNSS to measure at 1 Hz using GPS, GLONASS, Galileo and SBAS constellations. Some of the contents of the output file are times of measurements, the value of the measured specific force for each of the three dimensional axes, three dimensional curvilinear coordinates (Latitude, Longitude, ellipsoidal height) in World Geodetic System 1984 (WGS84), and the magnetic headings. Units of measurements are as specified in the manufacturer's manual.

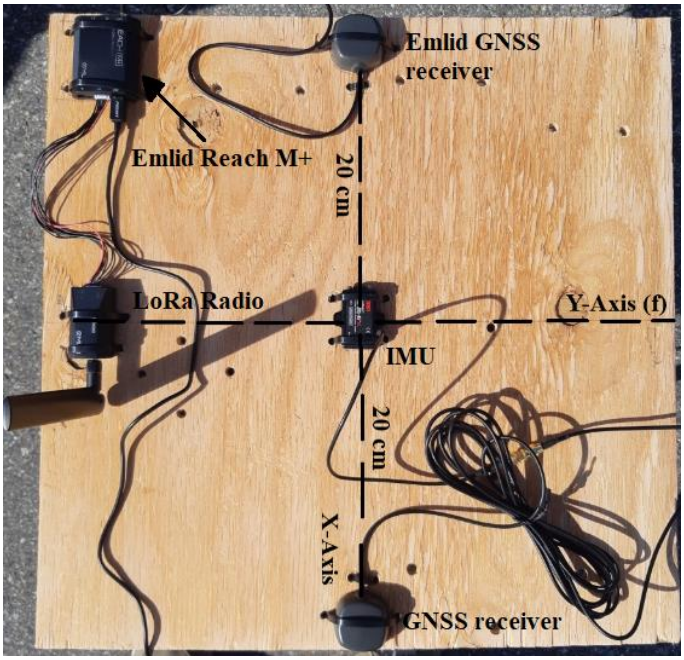

Figure 1 A picture showing the platform setup with the instruments strapped down to it.

4.1 Data Pre-processing

The data pre-processing phase involves transforming derived GNSS curvilinear coordinates to Universal Transverse Mercator (UTM) zone 10 coordinates. This is done by using the WGS84 ellipsoidal parameters and performing rigorous calculations. Converting the curvilinear coordinates into UTM equivalent is an important step before the integration of the IMU measurements; it transforms the coordinates to a common coordinate frame suitable for the integration of the IMU measurements. In one epoch (one second), 50 measurements in

both inertial sensors were collected. These values are to be averaged for the respective axes in order to get a reliable measurement between one position and the next.

5. PROCESSING ALGORITHM

The algorithm for processing the recorded INS and GNSS data is based on loosely-coupled Kalman Filtering procedure. This is a type of dynamic least squares method that calculates the optimal solution and its error estimates using an iterative weighted method.

5.1 IMU Data Processing

The IMU data processing algorithm is given as follows.

1. Correct each epoch for the averaged accelerometer measurements in each a_x, a_y in the *x* and *y* axes directions, respectively, for the systematic bias (initial bias error) (b_{ai}) in the accelerometer sensor. This is expressed in Equations (1) and (2).

$$\overline{a}_x = (a_x + b_{ai}) \quad (1)$$
$$\overline{a}_y = (a_y + b_{ai}) \quad (2)$$

   where $\overline{a}_x$ and $\overline{a}_y$ are the corrected accelerometer values in the x- and y- axes, respectively.
2. Rotate the corrected accelerometer values to the local geodetic frame (navigational frame) in order to be able to relate them to the UTM coordinate (*E*, *N*) system, where *E* is for easting and *N* for northing. This is expressed in Equations (3) to (5) as

$$\overline{a}_E = \overline{a}_x sin\psi + \overline{a}_y cos\psi \quad (3)$$
$$\overline{a}_N = \overline{a}_x cos\psi - \overline{a}_y sin\psi \quad (4)$$

   where

$$\psi = \psi_m - Grid\ Declination \quad (5)$$

   ψ is the corrected heading between true north and body frame x-axis
   ψ_m is the raw heading between true north and body frame x-axis, measured with the magnetometer of the IMU
   $Grid\ Declination$ is the angle between magnetic north and grid north obtained from the Natural Resources of Canada (2019)
   $\overline{a}_E$ is the rotated corrected accelerometer value in the easting (*E*) direction
   $\overline{a}_N$ is the rotated corrected accelerometer value in the northing (*N*) direction
3. Performing the error propagation on the rotated corrected accelerometer values to produce their respective standard deviations, as given in Equations (6) and (7)

$$\sigma_{\overline{a}_E} = \sqrt{(sin\psi)^2\sigma_{b_a}^2 + (a_x cos\psi - a_y sin\psi)^2\sigma_\psi^2 + (cos\psi)^2(\sigma_{b_a}^2)} \quad (6)$$

$$\sigma_{\overline{a}_N} = \sqrt{(cos\psi)^2\sigma_{b_a}^2 + (a_x cos\psi + a_y sin\psi)^2\sigma_{\psi}^2 + (-sin\psi)^2(\sigma_{b_a}^2)} \quad (7)$$

where

σ_{b_a} is the bias instability of the accelerometer sensor
σ_{ψ} is the accuracy of the magnetic heading

5.2 Kalman Filter

The loosely-coupled Kalman Filtering procedure is used in integrating the IMU and the GNSS measurements. The state vector, $\hat{x}_k$, is the desired filtered solution at time t_k containing position and velocity in easting and northing. The Kalman filtering algorithm uses the previously adjusted state vector $\hat{x}_{k-1}$to predict the state vector of the next k[th] point as (Ogundare, 2019)

$$\overline{x}_k = H\overline{x}_{k-1} + B_{k-1}u_{k-1} \quad (8)$$

and the corresponding predicted cofactor matrix as

$$Q_{\overline{x}_k} = HQ_{\hat{x}_{k-1}}H^T + Q_{w_{k-1}} \quad (9)$$

where
H is the state transition matrix from t_{k-1} to t_k
B_{k-1} is the control input matrix representing additional information that aren't related to the state itself such as pushing down on the throttle to accelerate
u_{k-1} is the vector of control inputs of the dynamic system such as breaking force
$Q_{\overline{x}_k}$is the covariance matrix of the predicted state vector at epoch *k*
$Q_{\hat{x}_{k-1}}$is the covariance matrix of the filtered state vector
$Q_{w_{k-1}}$ is the cofactor matrix of noisy control inputs, which can be determined as

$$Q_{w_{k-1}} = b_a^2(B_{k-1}B_{k-1}^T) \quad (10)$$

In this study, the the prediction equations are formulated by taking the double integral of acceleration to determine the position vector and a single integral of acceleration to obtain the velocity. The predicted state vector can be given as

$$\overline{E}_k = \hat{E}_{k-1} + \Delta t * \hat{v}_{E_{k-1}} + \frac{1}{2}\overline{a}_{E_{k-1}} * \Delta t^2 \quad (11)$$
$$\overline{N}_k = \hat{N}_{k-1} + \Delta t * \hat{v}_{N_{k-1}} + \frac{1}{2}\overline{a}_{N_{k-1}} * \Delta t^2 \quad (12)$$
$$\overline{v}_{E_k} = \hat{v}_{E_{k-1}} + \overline{a}_{E_{k-1}} * \Delta t \quad (13)$$
$$\overline{v}_{N_k} = \hat{v}_{N_{k-1}} + \overline{a}_{N_{k-1}} * \Delta t \quad (14)$$

where

$\bar{E}_k, \bar{N}_k$ are respectively the predicted easting and northing for the next epoch *k*;
$\hat{E}_{k-1}, \hat{N}_{k-1}$ are respectively the filtered easting and northing for the previous epoch *k-1*;
$\bar{v}_{E_k}, \bar{v}_{N_k}$ are respectively the predicted velocity components in the easting and northing at the next epoch *k*;
$\hat{v}_{E_{k-1}}, \hat{v}_{N_{k-1}}$ are respectively the filtered velocity components in the easting and northing at the previous epoch *k-1*;
$\bar{a}_{E_{k-1}}, \bar{a}_{N_{k-1}}$ are respectively the corrected accelerometer values in the easting and northing at the previous epoch k-1 based on Equations (4) and (5).

The state transition matrix, H, is determine by finding the jacobian equations of the prediction Equations (11) – (14) as

$$H = \begin{bmatrix} 1 & 0 & \Delta t & 0 \\ 0 & 1 & 0 & \Delta t \\ 0 & 0 & 1 & 0 \\ 0 & 0 & 0 & 1 \end{bmatrix} \quad (15)$$

The corrections to the predictions made using Equations (11) – (14) are made by using the measurement model and applying the Kalman Gain. The measurement equations can be formulated as

$$\hat{l}_{E_k} = \hat{E}_k \quad (16)$$
$$\hat{l}_{N_k} = \hat{N}_k \quad (17)$$
$$\hat{l}_{v_{E_k}} = \hat{v}_{E_k} \quad (18)$$
$$\hat{l}_{v_{N_k}} = \hat{v}_{N_k} \quad (19)$$

Equations (16) – (19) are the direct measurements of the state vector by the GNSS, which can be expressed generally as

$$l_k = A_k \hat{x}_k + e_k \quad (20)$$

where
A_k is the design matrix found by deriving the jacobian of measurement equations with respect to the state vector;
l_k is a vector of direct measurements given in Equations (16) – (19);
e_k is random noise, which is usually set to 0.

The cofactor (Q_{l_k}) of measurements is constructed by propagating the errors associated with measurements in the prediction equations, as

$$Q_{l_k} = \begin{bmatrix} \sigma^2_{\overline{E}_k} & 0 & 0 & 0 \\ 0 & \sigma^2_{\overline{N}_k} & 0 & 0 \\ 0 & 0 & \sigma^2_{\overline{v}_{E_k}} & 0 \\ 0 & 0 & 0 & \sigma^2_{\overline{v}_{N_k}} \end{bmatrix} \quad (21)$$

where
$\sigma^2_{\overline{E}_k}$ and $\sigma^2_{\overline{N}_k}$ are the variances of the measured easting and northing coordinates, respectively;
$\sigma^2_{\overline{v}_{E_k}}$ and $\sigma^2_{\overline{v}_{N_k}}$ are the variances of the measured velocity components in the easting and northing, respectively.

The Kalman Gain (K_k), which is to be used in weighting the IMU and GNSS solutions in arriving at the filtered state vector can be given (Ogundare, 2019, p. 573) as

$$K_k = Q_{\overline{x}_k} A_k^T (A_k Q_{\overline{x}_k} A_k^T + Q_{l_k})^{-1} \quad (22)$$

The Kalman Gain is used to update the predicted state vector in order to obtain the filtered state vector ($\hat{x}_k$) and filtered covariance matrix ($Q_{\hat{x}_k}$) of the filtered state vector, which can be expressed as

$$\hat{x}_k = \overline{x}_k + K_k(l_k - A_k \overline{x}_k) \quad (23)$$

$$Q_{\hat{x}_k} = (I - K_k A_k) Q_{\overline{x}_k}^T \quad (24)$$

where I is a 4x4 identity matrix. These filtered matrices are used in the next prediction and the same process of prediction and updating are repeated in a similar version.

6. ANALYSIS OF RESULTS

The loosely-coupled Kalman filtering uses the direct GNSS measurements and their covariance matrices in Equations (23) and (24) to obtain filtered state vectors. Two approaches are followed in orienting the track of the navigating vehicle in this study: using the immediate past bearing estimates from GNSS measurements for subsequent iteration and using the values based on magnetometer headings given in Equation (5). The general results showed that the loosely-coupled Kalman Filter algorithm favoured the accuracies of the IMU more than the GNSS solutions. Figure 2 shows the filtered coordinates obtained from using the bearings from the previous GNSS point and the next; the filtered coordinates based on the use of magnetometer headings approach are given in Figure 3.

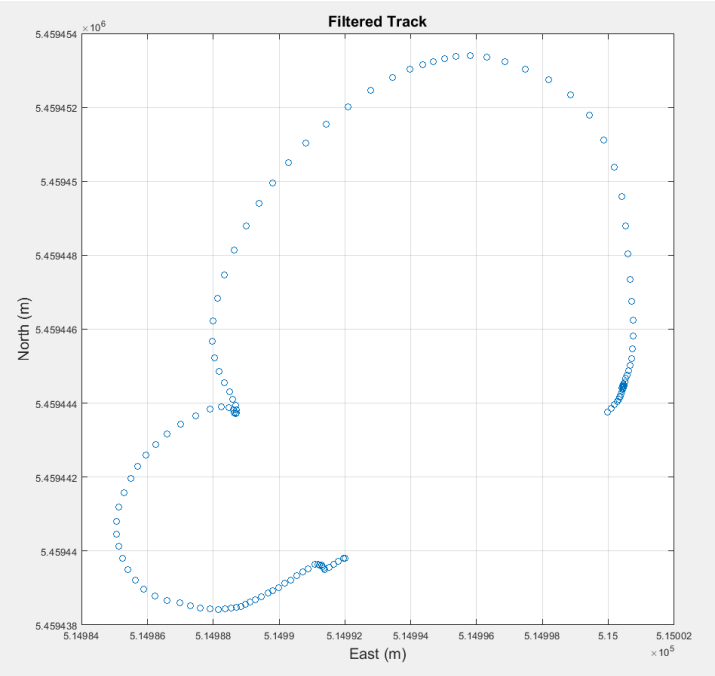

Figure 2 Loosely-coupled Kalman filtered coordinates of the track of navigating vehicle based on the GNSS bearing estimate approach.

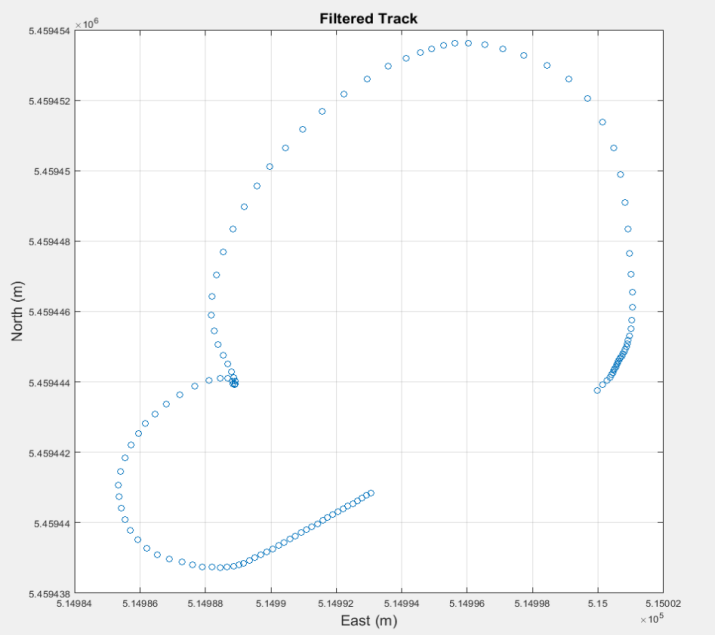

Figure 3 Loosely-coupled Kalman filtered coordinates of the track of navigating vehicle based on the magnetometer heading approach.

It can be seen from Figure 2 and Figure 3 that the plots are identical. From these two figures, it can be said that the headings based on magnetometer measurements are consistent with those based on GNSS approach within the accuracy specification of GNSS measurements.

Figure 4 shows the standard deviations of the predicted positions and velocities divided into separate axes for the case referring to a case where the initial positional standard deviation of 5 meters estimated for the GNSS single frequency solution is used. In this case, the predicted standard deviation for position is expected to decrease to sub-meter level and stabilize. The increased accuracy is due to the high level of accuracy that the IMU offers. In this case, the Kalman Filter relies more heavily on the IMU's measurements than the measurements from GNSS, so coordinates derived from IMU measurements are treated to be closer to the true value. On the other hand, the predicted standard deviations of the velocity components decrease in accuracy, although not significantly, and stabilize within ten seconds.

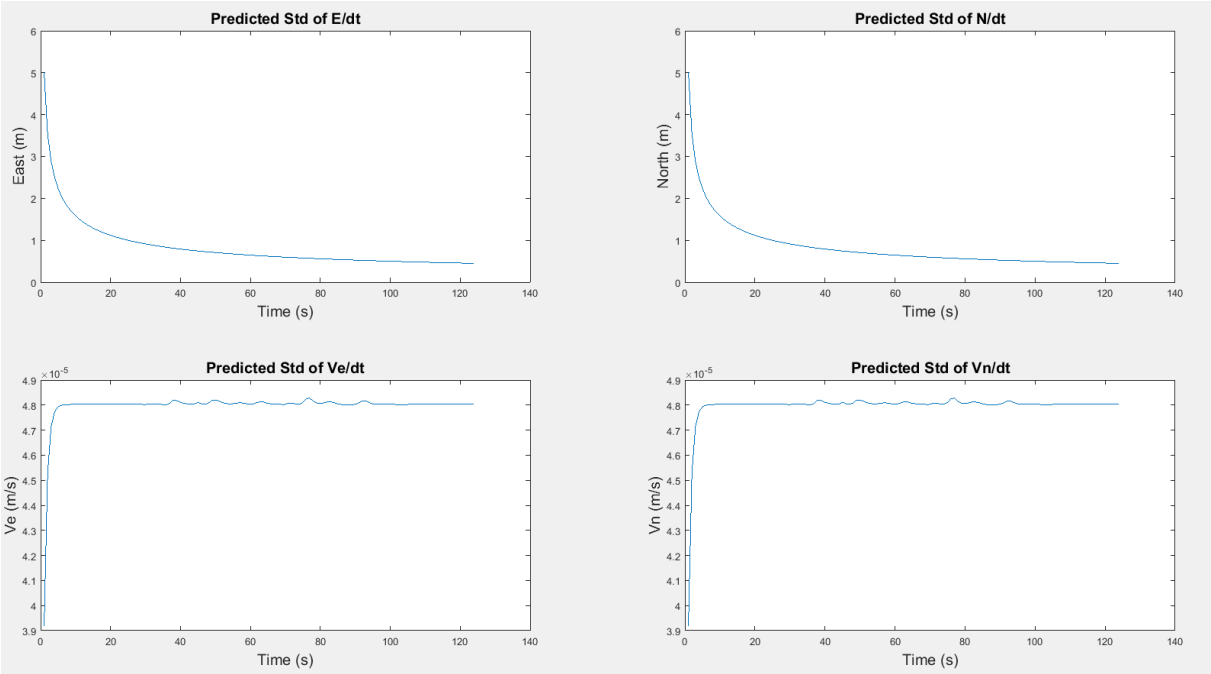

Figure 3 Plot of standard deviations of the predicted state vector solutions over time, t (in seconds) (Initial positional standard deviation of 5 meters used).

Figure 5 shows the filtered standard deviations of the state vector solution (position and velocity) for the case where the initial positional standard deviation of 3.5 meters estimated for the GNSS single frequency solution is used. As time progresses, the filtered standard deviations of position improve and stabilize. From an initial 3.5 meter standard deviation in filtered position, it improves to approximately half a meter in about two minutes. The standard deviation in filtered velocity stabilizes as expected with a magnitude of approximately half of what the predicted values were.

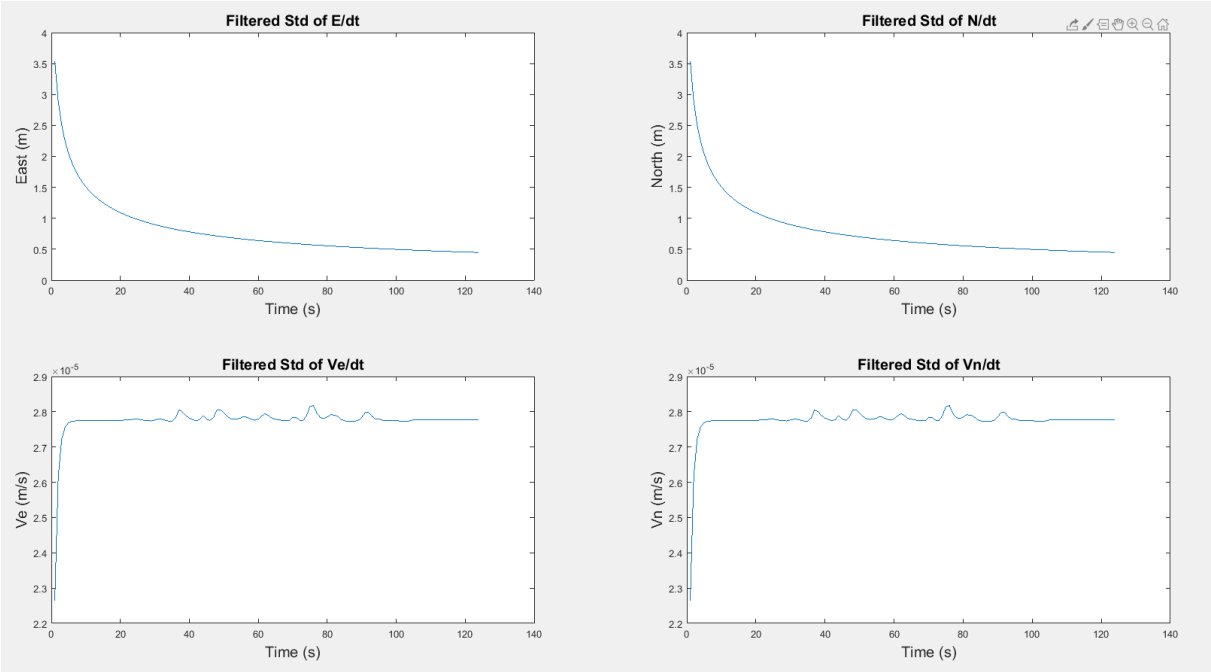

Figure 4 Plot of the standard deviations of the filtered state vector solutions over time, t (in seconds) (Initial positional standard deviation of 3.5 meters used).

Figure 6 shows the difference in magnitude between computed filtered coordinates and GNSS UTM coordinates. In the Easting axis, the maximum difference is about 28 meteres and in the Northing axis, the maximum difference is about 38 meters. Within the first 20 seconds, differences between filtered coordinates and GNSS coordinates were less than 5 meters, which is suitable for vehicular navigation.

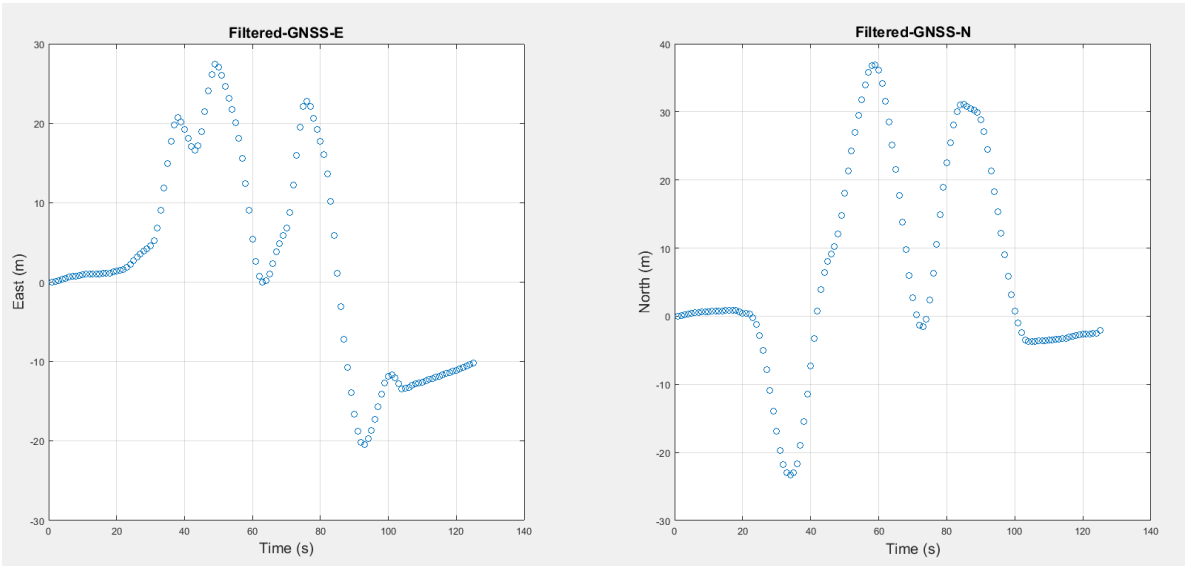

Figure 5 Plot of the differences between filtered coordinates and GNSS UTM coordinates.

7. CONCLUSION

The results of integration of Lord MicroStrain 3DM-GX5-10 IMU with single frequency multi-constellation GNSS obtained in this report did not compare very well with those from GNSS only. The analyses, however, showed that the integration can still be relied on at the moments of satellite downtime. Due to limited resources, a longer track could not be run to assess the quality of the INS used. It is recommended that those who wish to further this work should consider integrating the two systems using a tightly-coupled method and implementing the more rigorous three-dimensional algorithm.

REFERENCES

El-Rabanny, A. (2006). *Introduction to GPS The Global Positioning System* (2nd ed.). (E. Kaplan and C. Hegarty, Eds.) Norwood, Massachusetts, United States of America: Artech House. Retrieved February 3, 2020

Farrell, J. A., & Barth, M. (1999). *The Global Positioning System & Inertial Navigation.* New York City, New York, United States of America: The McGraw-Hill Companies, Inc. Retrieved February 3, 2020

Grewal, M. S., Weill, L. R., & Andrews, A. P. (2001). *Global Positioning Systems, Inertial Navigation, and Integration.* New York City, New York, United States of America: John Wiley and Sons, Inc. Retrieved February 3, 2020

Hofmann-Wellenhof, B., & Moritz, H. (2006). *Physical Geodesy* (2nd ed.). Graz, Austria: SpringerWienNewYork. Retrieved February 6, 2020

Natural Resources Canada. (2019). *Tools and Applications*. February 22. https://www.nrcan.gc.ca/maps-tools-and-publications/tools/geodetic-reference-systems-tools/tools-applications/10925#ppp

Ogundare, J. O. (2019). *Understanding Least Squares Estimation and Geomatics Data Analysis* (1st ed.). Hoboken, New York, United States of America: John Wiley and Sons, Inc. Retrieved February 3, 2020

BIOGRAPHICAL NOTES

Chadrick Ly is a Bachelor of Science graduating student of the Geomatics program at the British Columbia Institute of Technology. He was awarded "The BC Land Surveyors Vancouver Island Group and Association of BC Land Surveyor Awards," for his excellent academic performance and leadership. He is a land surveyor in training at Target Land Surveying and currently works towards obtaining his commission as a professional land surveyor in BC.

John Ogundare is a practising professional geomatics engineer in British Columbia, Canada; an instructor of Geomatics engineering at the British Columbia Institute of Technology, Canada; and an author of two books published by Wiley & Sons, Inc., Hoboken: *The Precision Surveying: The Principles and Geomatics Practice* and *Understanding Least Squares Estimation and Geomatics Data Analysis*. He has been in the field of geomatics for over thirty years in Africa and Canada. Dr. Ogundare has been a representative of and a special examiner for the Canadian Board of Examiners for Professional Surveyors (CBEPS) for over ten years.

CONTACTS

Mr. Chadrick Ly
British Columbia Institute of Technology
SE16 – 3700, Willingdon Avenue
Burnaby
CANADA
Cell phone: 1-778-872-8219
Email: chad-tl@hotmail.com

Dr. John Ogundare, PEng.
British Columbia Institute of Technology
SW2-317 3700, Willingdon Avenue
Burnaby, BC
CANADA
Tel. 1-604-431-4944
Email: john_ogundare@bcit.ca
Web site: www.bcit.ca